Parameter Estimation of Organic Photovoltaic Cells – A Three-Diode Approach Using Wind-Driven Optimization Algorithm

Derick Mathew [ID], J. Prasanth Ram [ID], Dhanup S. Pillai [ID], *Member, IEEE*, Young-Jin Kim [ID], *Senior Member, IEEE*, D. Elangovan, *Member, IEEE*, Antonino Laudani [ID], *Member, IEEE*, and Apel Mahmud [ID], *Senior Member, IEEE*

Abstract—**Modeling a reliable electrical equivalent circuit to simulate the output *I–V* characteristics of organic solar PV (OPV) cells still prevails as a challenging task. This is because, estimating unknown parameters from the transcendental current equation determining the nonlinear OPV characteristics is extremely difficult. More importantly, predicting the parameters for dynamic changes in irradiation profile demands reliable optimization-based models. Therefore, this article proposes the application of adaptive wind-driven optimization (WDO) algorithm for a three-diode electrical equivalent model to estimate the OPV circuit parameters. Application of WDO algorithm has produced precise PV parameters to reproduce the exact *I–V* characteristics. In particular, the ability to replicate the kink effect in OPV characteristics is a noticeable improvement. Compared to its counterparts, various factors that enable WDO to enhance its compatibility towards nonlinear OPV modeling are: i) unique velocity update strategy via Coriolis and Gravitational forces, ii) excellent tradeoff between exploration and exploitation of control variables, iii) adaptive capability to maintain solutions within the search space even if the limits are breached, and iv) easiness in parameter tuning. For the validation, extensive testing has been conducted to reproduce the widely used characteristics of nav100 OPV cell at various operating conditions. Quantitatively, WDO method showcases excellent accuracy with an individual absolute error value in the order of 10^{-6} and convergence within the first 50 iterations itself, demonstrating its supremacy to solve OPV parameter identification problem.**

Index Terms—**Modeling, organic PV (OPV), parameter estimation, photovoltaic (PV), wind-driven optimization (WDO).**

Derick Mathew is with the Department of Electrical Engineering, UKF College of Engineering and Technology, Kerala 691302, India (e-mail: derickmathew1@gmail.com).

J. Prasanth Ram is with Energy Systems Lab, Department of Electrical Engineering, Pohang University of Science and Technology, Pohang 37666, South Korea (e-mail: drjppram@postech.ac.kr).

Dhanup S. Pillai is with the National University of Singapore, Singapore 11574, Singapore (e-mail: dhanup.research@gmail.com).

Young-Jin Kim is with Energy Systems Lab, Department of Electrical Engineering, Pohang University of Science and Technology, Pohang 37666, South Korea, and also with the Institute for Convergence Research and Education in Advance Technology, Yonsei University, Seoul 03722, South Korea (e-mail: powersys@postech.ac.kr).

D. Elangovan is with the Technology Information Forecasting and Assessment Council Core, School of Electrical Engineering, Vellore Institute of Technology, Vellore 632014, India (e-mail: elangovan.devaraj@vit.ac.in).

Antonino Laudani is with the Department of Engineering, Roma Tre University, I-00146 Roma, Italy (e-mail: alaudani@uniroma3.it).

Apel Mahmud is with the School of Engineering, Faculty of Science Engineering and Built Environment, Deakin University, Geelong, VIC 3220, Australia (e-mail: apel.mahmud@deakin.edu.au).

Color versions of one or more figures in this article are available at https://doi.org/10.1109/JPHOTOV.2021.3129874.

Digital Object Identifier 10.1109/JPHOTOV.2021.3129874

NOMENCLATURE

R_s	Series resistance.
V_D	Diode voltage.
R_{P1}, R_{P2}	Parallel resistance.
I_{01}, I_{02}, I_{03}	Diode reverse saturation currents.
n_1, n_2, n_3	Diode ideality factors.
I_{irr}	Initial photon current.
V_T	Terminal voltage.
V_{OC}	Open circuit voltage.
F_{PG}	Pressure gradient force.
F_F	Frictional force.
F_G	Gravitational force.
F_C	Coriolis force.
α	Frictional coefficient.
ρ	Resultant of air density.
$\overrightarrow{u}$	Wind velocity vector.
δV	Finite volume present in air parcels.
$\vec{g}$	Gravitational vector.
θ	Angle of deflection.
$\vec{u}_{C_j}^k, u_{new_j}^k$	Velocity of previous and current iteration.
$\vec{y}_{C_j}^k, y_{new_j}^k$	Position of air parcels in previous and current iteration.

Abbreviations

IAE	Individual absolute error.
BFA	Bacterial foraging algorithm.
FPA	Flower pollination algorithm.
BPFPA	Bee pollinated FPA.
BIPV	Building Integrated PV.
RMSE	Root-mean-square error.
SSE	Sum of squared error.
GA	Genetic algorithm.

I. INTRODUCTION

FACILITATED by wide bandgap operation, flexible design feature of organic solar PVs (OPVs) has enabled the PV to convert invisible ultraviolet and infrared light energy to electrical energy [1]. Particularly, the advantages like i) low cost manufacturing, ii) light weight nature, and iii) increased efficiency have made OPVs preferable to its predecessors [2], [3]. Besides, layer-based fermentation in OPV is an indispensable technology for BIPV applications. However, unlike silicon-based cells, commercialization of OPVs has not been that substantial. This is because, researchers use different active and interlayers for designing OPV, which makes it difficult to characterize an accurate model [4]. Thus, it is important to develop a suitable modeling technique capable of attaining precise OPV parameters for realistic I–V curve characterization.

PV modeling and its characterization started with an electrical equivalent circuit comprising of diodes and resistors connected in series-parallel fashion [5]. Later, with the motivation to improve accuracy, two diode model has been introduced with the addition of an external diode to the classical one diode model. To replicate the conventional PV characteristics optimization methods are used. Among many, few methods like bird mating optimizer [6], fireworks algorithm [7], differential evaluation [8], bacterial foraging algorithm [9], flower pollination algorithm (FPA) [10], and bee pollinated FPA [11] have been successfully proposed in literature. Detailed study on PV modeling using optimization techniques can be found in [12] and [13]. However, the classical one and two diode models are not compatible for OPV characterization as these models fail to emulate the kink effect in OPV output characteristics [14]. Note that "kink effect" refers to the inherent "S-shape" in the I–V characteristics of OPV cells in contrast to the conventional PV cells. For enhanced reading, detailed discussions on kink effect in OPVs are provided in [4] and [15].

For OPV modeling, modifications are made in the conventional one diode model by incorporating additional diodes and resistors in parallel [16], [17]. However, these models were also unsuccessful to replicate the actual S-shape behavior of OPV. The accurate reproduction of I–V characteristics was first obtained in [18] by integrating a resistor in parallel to the second diode. Though the model was successful, the charge accumulation process in the modified circuit makes it voltage dependent (while PV must be current dependent and the current values are estimated according to the voltage value of experimental data). Though new modifications were proposed to the same circuit in [15] and [19] as an alternative to [18], the charge accumulation problem persists with the modified versions as well. To solve the issue effectively, a new electrical equivalent circuit is developed in [20] with two antiparallel diodes connected in parallel to the shunt resistance. Furthermore, the method is also effective to reproduce the actual S–shaped I–V characteristics. However, the model equation derived using the electrical equivalent circuit is transcendental and, therefore, requires approximations in the dataset to identify accurate OPV parameters as for some conventional parameter estimation techniques like in [21] and [22].

To solve the nonlinearity and approximations with OPV electrical equivalent circuit, a new solution via lambert — W is proposed in [23] and [24]. The method utilizes a one diode model with a series resistor, which is proficient to estimate PV parameters accurately via curve fitting approach. Being the predecessor, the method inspired many researches to accomplish nearly accurate curve fit in OPV [15], [25], and [26]. Among those, Romero *et al.* [19] and Jain and Kapoor [25] provided valuable findings since the mathematical equation proposed by these works use the reverse two-diode model for curve fit attainment. However, as discussed earlier, Romero *et al.* [19] used a voltage dependent expression as a function of current and, therefore, becomes less reliable for estimating PV parameters. While double-diode model approximations performed in [15] and [18] reduce the transcendental nature of mathematical equations, the adopted procedure relies on many assumptions and approximations, making them less consistent for parameter estimation during different operating conditions. The three-diode model for OPV was first proposed by De Castro [26] and Roland *et al.* [27]. The circuit proposed a reassembly of [20] to model the S-shaped OPV characteristics. Interestingly, the effect of R_s is neglected in the modeled parameter relationship on I–V characteristics. Also, the error analysis and curve fit are only presented for specific illuminance conditions. Identically, Laudani *et al.* [28] tested the same model for various irradiances and their respective parameters are identified using the Genetic Algorithm (GA). Although the three-diode model establishes itself as a standard to deliver S-shaped OPV, GA approach still needs improvement to avoid convergence to local optima. Also, initialization with huge population, complex mutation and crossover steps increase the iteration count and computation time.

In the abovementioned context, this article proposes an adaptive wind-driven optimization (WDO) algorithm-based modeling approach for estimating the unknown parameters of the three-diode OPV model. Unlike other metaheuristic optimization techniques, WDO is a less population dependent and computationally fast technique that utilizes four various velocity update processes for a single particle [29], [30]. More importantly, the proposed WDO approach utilizes adaptive velocity generation strategy to escape from local minimums and reach global optimal regions. In addition, WDO allows us to efficiently program both exploration and exploitation processes via its control variables. More importantly, tuning control parameters of WDO is fairly easy compared to previously discussed GA method. Thus, the inherited tradeoff between global exploration, exploitation and computational efficiency is envisaged to make WDO distinct from other optimization techniques and compatible for OPV parameter estimation problem. As it is, the compatibility of WDO OPV parameter identification is comprehensively studied and applied to three-diode modeling in this article. For validation, four different datasets have been considered and their corresponding I–V characteristics are presented. Furthermore, the individual error analysis is also demonstrated to showcase the computational efficiency and accuracy. The important contributions of this article is summarized in the following.

1) A comprehensive three-diode OPV modeling is made to reproduce the nonlinear kink effect.
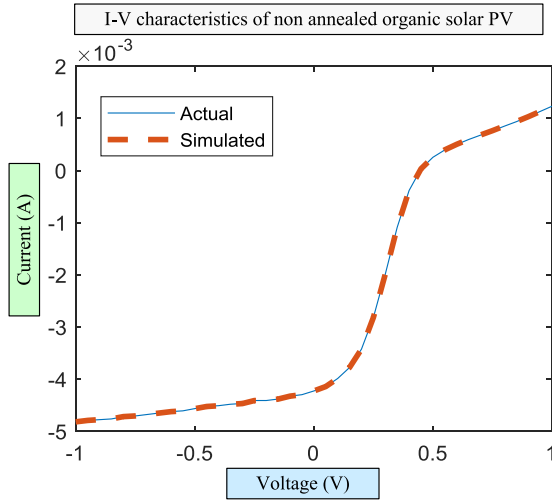2) The unknown PV parameters of three-diode model are obtained using WDO algorithm.

Fig. 1.   *I–V* characteristic of nonannealed organic solar PV in dark irradiation condition.

3) The ability of WDO to keep alive the arbitrariness in control variables gives hasty convergence to global solutions.
4) Accurate curve fit is obtained even at lower insolation cases which illustrates the competence of WDO for OPV parameter estimation.

II. ORGANIC SOLAR PV MODELING

PV modeling represents the electrical equivalent circuit to simulate *S*-shape characteristics of an organic PV module. For this study, an organic film fabricated on cleaned ITO-coated glass coated with 50 nm of PEDOT: PSS (Aldrich, conductivity 1 S/cm^{-1}) acts as anode and similarly, 50 nm of Al act as a cathode. Besides, bilayered – Poly [2- methoxy - 5- (2-ethylhexyloxy)-1, 4-phenylene-vinylene] (MEH-PPV, $M_n =$ 40 000–70 000, Aldrich) is made to act as an electron donor and fullerene C60 (>99.95%, SES Research) acts as an acceptor. It is important to mention here that the material characterization and fabrication is performed in inert N$_2$ atmosphere. Detailed specification of the model and its preparations can be referred to [18] and [31]. For understanding, the representation of a simple *S*-shaped nonannealed *I–V* characteristic of prepared sample is presented in Fig. 1. From the characteristic, it is observed that the *I–V* curve has a unique *S*-shaped structure, and its behavior cannot be simulated by the conventional diode model. Furthermore, the key observations pertinent to the curve that may help to formulate the actual electrical equivalent model are: i) the characteristics are similar to crystalline silicon model till V_{oc}, ii) the curve becomes linearly increasing after V_{oc}, to create kink effect / *S*-shape behavior in the characteristics, and iii) after *Voc*, the current change becomes negligible with the change in voltage and subsequently creates a kink effect in the *I–V* characteristics. The observation indeed illustrates the need for modifications in the one diode model to simulate the kink effect of OPV. Tada [32] developed a reverse two diode model to simulate the characteristic. However, the kink effect will not be accurate when the sample is tested for various irradiations.
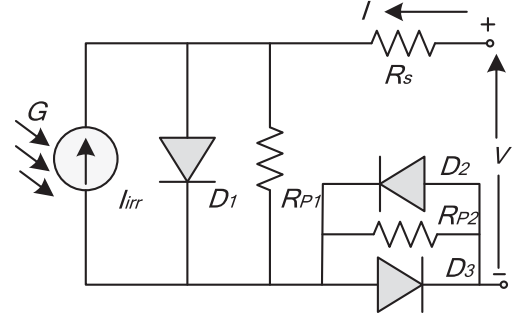

Fig. 2.   Representation of a three-diode PV model.

Hence, this article follows the three-diode model presented in [28], which seems to be most compatible. Furthermore, curve fit analysis is performed for four various temperatures as 120 °C, 150 °C, 180 °C, and 200 °C annealed for 5 min. Besides, the annealed samples at each temperature are tested at various insolation changes to check the accuracy of modeling. For understanding, the annealed models corresponding to temperature 120 °C, 150 °C, 180 °C, and 200 °C are represented as "a120Cmin", "a150Cmin", "a180Cmin", and "a200Cmin", respectively. Electrical equivalent circuit of three-diode model is presented in Fig. 2. The three-diode model in figure has diodes D_2, D_3, and parallel resistance (R_{P2}) in addition to one diode model to create the kink effect in OPV. All elements represent the series resistance and hence, the influence of actual R_s is neglected. Detailed explanations for the negligence of R_s can be found in [27]. For modeling, let the voltage across the diodes be termed as V_{D1}, V_{D2}, and V_{D3}. Furthermore, the circuit clearly states that voltage $V_{D2} = -V_{D3}$, then using Kirchhoff's voltage law, the equation can be formulated as

$$V = V_{D1} - V_{D2} = V_{D1} + V_{D3}. \tag{1}$$

The voltage across diode as a function of current can be written as follows:

$$V_{D1} = (I + I_{irr} + I_{01}) \; R_{p1}$$
$$- n_1 V_T W \left(\frac{I_{01} R_{P1}}{n_1 V_T} \exp \left(\frac{(I + I_{irr} + I_{01}) R_{p1}}{n_1 V_T} \right) \right). \tag{2}$$

Since, expressing V_{D2} is difficult due to the presence of diode D_3. Alternatively, it is possible to obtain current (I) as a function of voltage V_{D2} and it is given as follows noting $V_{D3} = -V_{D2}$:

$$I = -\frac{V_{D2}}{R_{P2}} - I_{02} \left(\exp \left(\frac{V - V_{D1}}{n_2 V_T} \right) - 1 \right)$$
$$+ I_{03} \left(\exp \left(\frac{V - V_{D1}}{n_3 V_T} \right) - 1 \right) \tag{3}$$

where I_{02} and I_{03} denote the reverse saturation currents, n_2 and n_3 denote the diode ideality factors, and V_T is the terminal voltage. From (1), the expression for V_{D2} can be given as

$V_{D2} = V - V_{D1}$ and, hence, (3) can be written as

$$I = \frac{V - V_{D1}}{R_{P2}} - I_{02}\left(\exp\left(\frac{V - V_{D1}}{n_2 V_T}\right) - 1\right)$$
$$+ I_{03}\left(\exp\left(\frac{V - V_{D1}}{n_3 V_T}\right) - 1\right). \qquad (4)$$

Now, the expression of V_{D1} can be applied to (4) to get the current equation as follows.

Thus, from the abovementioned equation, it can be concluded that current values can be obtained in the relation of voltage and nine parameters are unknown R_{P1}, R_{P2}, I_{01}, I_{02}, I_{03}, n_1, n_2, n_3, and I_{irr}. These parameters are identified using WDO procedure and the procedure is discussed in the following section.

III. PROBLEM FORMULATION

Parameter estimation in solar PV optimizes the unknown parameters formulated in (5) shown at the bottom of this page, to simulate the I–V characteristics of OPV. Furthermore, by using these parameters, the points in the I–V curves are simulated and their degree of closeness is verified with experimental data (curve fit approach). Note that in this article, WDO is used to find the PV parameters. It is worth to mention here that root-mean-square error via curve fit is adopted in this article to test the solution quality. The procedure to arrive at the formulation of objective function is discussed as follows. As an initial step, the individual absolute error is calculated as an absolute of difference between the actual and simulated data. Expression for individual absolute error as a function (V_m, I_m, x) is given in

$$f_i (V_m, I_m, x) = \text{IAE} = abs (I_{\text{actual}} - I_{\text{simulated}}) \qquad (6)$$

where x is the function of R_{P1}, R_{P2}, I_{01}, I_{02}, I_{03}, n_1, n_2, n_3, and I_{irr} with I_{actual}' as the experimental data and $I_{\text{simulated}}$ as the estimated values from simulation. The sum of squared error is determined as given in

$$\text{SSE} = \sum_{i=1}^{N} \text{IAE}_i^2 \qquad (7)$$

where N is the number of points in the I–V curve and the RMSE is determined as follows:

$$\text{RMSE} = \sqrt{\frac{1}{N}\text{SSE}}. \qquad (8)$$

The extraction of parameters R_{P1}, R_{P2}, $I_{01}, I_{02}, I_{03}, n_1, n_2$, n_3, and I_{irr} is crucial in optimization since it avoids convergence to local optima. Identified as one of the best methods to handle multidimensional problems, WDO procedure is used here. Having four various velocity updating process, the WDO process is expected to have better results for the parameter estimation problem.

A. WDO Algorithm – Basics

Inspired from earth science, a new WDO is proposed and tested for multimodal problems. The coherent idea behind WDO process is to equalize the horizontal imbalances in air pressure. As the earth surface has huge temperature variations, horizontal imbalances do occur in movement of air. Furthermore, it is always seen that wind movement is accompanied by infinitesimal air particles exerted by earth gravitational field g. Due to the gravitational field, a force is created to move the air parcels from high-pressure regions to low-pressure regions. Graphical representation of air parcels moving in horizontal imbalances are shown in Fig. 3(a). The mathematical representation of force acting on wind parcel can be represented with the help of Newton's second law of motion in Lagrangian description. According to the law, the algebraic sum of applied force (F_t) is an equivalent to the result of acceleration in air parcel $(\overrightarrow{a})$ with the air density (ρ) associated to it, i.e.,

$$\rho. \overrightarrow{a} = \sum \overrightarrow{F_t} \qquad (9)$$

where the force (F_t) is the combination of four forces that include pressure gradient force (F_{PG}), frictional force (F_F), gravitational force (F_G), and Coriolis force (F_C). Note that these forces are crucial to create velocity for the air parcels to reach for global regions. Since, the movement in pressure gradient force (F_{PG}), as shown in Fig. 3(b), is a result of finite volume present in air parcels (δV), it can be mathematically represented in

$$\overrightarrow{F_{\text{PG}}} = -\overrightarrow{\Delta P}.\delta V. \qquad (10)$$

$$I = \frac{V - \left[(I+I_{irr}+I_{01})R_{p1} - n_1 V_T W\left(\frac{I_{01}R_{P1}}{n_1 V_T}e^{\frac{(I+I_{irr}+I_{01})R_{p1}}{n_1 V_T}}\right)\right]}{R_{P2}}$$
$$-I_{02}\left(e^{\frac{V - \left[(I+I_{irr}+I_{01})R_{p1} - n_1 V_T W\left(\frac{I_{01}R_{P1}}{n_1 V_T}e^{\frac{(I+I_{irr}+I_{01})R_{p1}}{n_1 V_T}}\right)\right]}{n_2 V_T}} - 1\right)$$
$$+I_{03}\left(e^{-\frac{V - \left[(I+I_{irr}+I_{01})R_{p1} - n_1 V_T W\left(\frac{I_{01}R_{P1}}{n_1 V_T}e^{\frac{(I+I_{irr}+I_{01})R_{p1}}{n_1 V_T}}\right)\right]}{n_3 V_T}} - 1\right) \qquad (5)$$
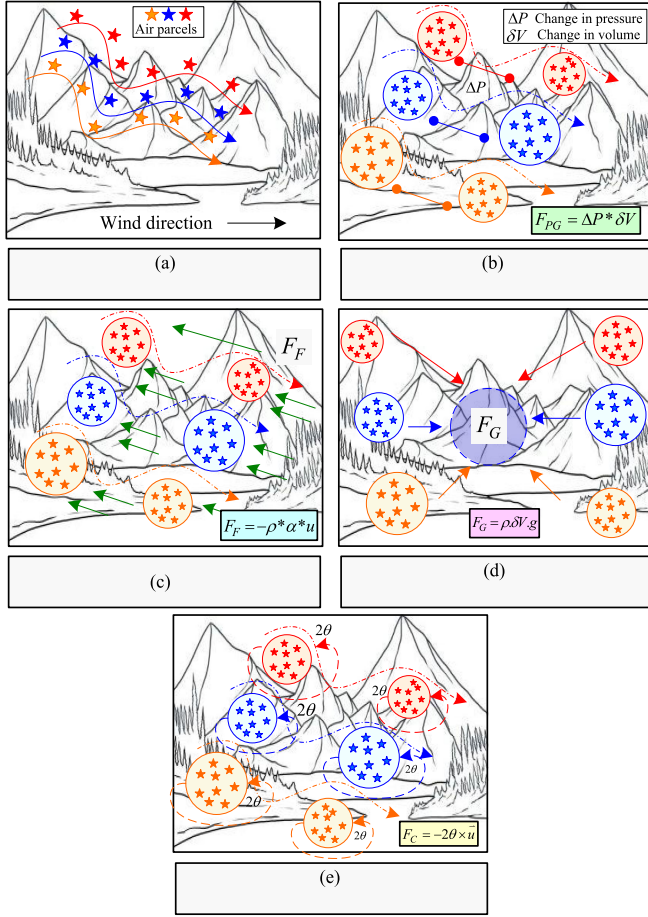
Fig. 3. Various forces acting on movement of air parcels on horizontal imbalances.

Frictional force (F_F), on the other hand acts in opposite direction to the pressure gradient force (F_{PG}), as shown in Fig. 3(c). Frictional force in general is resultant of air density (ρ), frictional coefficient (α), and wind velocity vector $(\vec{u})$. Hence, the mathematical representation can be given as follows:

$$\overrightarrow{F_F} = -\rho \, \alpha \, \vec{u}. \tag{11}$$

To pull the particles towards the center of earth, gravitational force is mandatory and it is characterized by a gravitational vector $(\vec{g})$. Visual representation of gravitational force can be referred in Fig. 3(d). The mathematical expression of resultant of air density and volume is given by

$$\overrightarrow{F_G} = \rho \, \delta V \, \vec{g}. \tag{12}$$

Since the rotational movement of earth has a great influence on the movement of air parcel, the Coriolis force that creates deflection in air is also considered in velocity update [see Fig. 3(e)]. The mathematical representation of Coriolis force associate with angle of deflection (θ) can be given as

$$\overrightarrow{F_C} = -2\theta \times \vec{u}. \tag{13}$$

Thus, the total force (F_t) on the movement of air parcels is given as a sum of pressure gradient force (F_{PG}), frictional force

(F_F), gravitational force (F_G), and Coriolis force (F_C) in

$$\rho \frac{\Delta \vec{u}}{\Delta t} = (\rho \delta V \vec{g})$$
$$+ (-\Delta P \delta V) + (-\rho \alpha \vec{u}) + (-2\theta \times \vec{u}). \tag{14}$$

As the nature of air parcels is dimensionless, change in volume (δV) is negligible. Furthermore, the effect of Δt is assumed to be 1 to make the velocity updation simple. The updated equation is given in

$$\rho \Delta \vec{u} = (\rho \vec{g}) + (-\Delta P) + (-\rho \alpha \vec{u}) + (-2\theta \times \vec{u}). \tag{15}$$

Rearranging the abovementioned equation by using pressure constant formula $\rho * P_c = R * T$, we get

$$\Delta \vec{u} = \vec{g} + \left(-\Delta P. \frac{RT}{P_c}\right) + (-\alpha \vec{u}) - \left(\frac{2\theta \vec{u} RT}{P_c}\right). \tag{16}$$

In the abovementioned equation, the gravitational vector is always served to pull the air parcels towards the center and, hence, it can be replaced as $|g| = (o - y_c)$ where y_c denotes the current position and similarly, the pressure gradient is intended to direct air parcels towards optimal location. Hence, it can be replaced as $|\Delta P| = (y_{\text{opt}} - y_c)$. Furthermore, it is important to maintain optimal pressure to avoid improper velocity update. Based on the velocity update, the air parcels are ranked for r in descending order and its mathematical representation considering k as air parcel and j as dimension can be given as follows:

$$\overrightarrow{u_{\text{new}_j}^k} = (1 - \alpha) \, \vec{u}_{C_j}^k - g \, y_{C_j}^k$$
$$+ \left(\begin{array}{c} \left|1 - \frac{1}{r^k}\right| . \\ \left(y_{\text{opt}_j}^k - y_{C_j}^k\right) RT \end{array}\right) + \left(\frac{2\theta \vec{u} RT}{r^k}\right) \tag{17}$$

where $\vec{u}_{C_j}^k$ and $u_{\text{new}_j}^k$ are the representation of velocity of previous and current iteration whereas $y_{\text{opt}_j}^k$ refers to the optimal position of air parcels. The position update of air parcel is given using

$$\overrightarrow{y_{\text{new}_j}^k} = \overrightarrow{y_{c_j}^k} + \left(\overrightarrow{u_{\text{new}_j}^k} \times \Delta t\right) \tag{18}$$

where $\vec{y}_{C_j}^k$ and $y_{\text{new}_j}^k$ are the representation of position for previous and current iterations. From the above discussion on WDO, the parameters to be tuned are found as *c, g, RT*, and α. Furthermore, these parameters are optimized and found using covariance matrix adaptation evolution strategy (CMAES) technique. It is noteworthy to mention here that velocity update of air parcels is allowed to move in the search space of $[-1, 1]$.

B. Applying WDO to OPV Parameter Estimation

To emulate the *I–V* characteristics of OPV, nine parameters R_{P1}, R_{P2}, I_{01}, I_{02}, $I_{03}, n_1 V_T, n_2 V_T$, $n_3 V_T$, and I_{irr} are needed to be found via the optimization procedure. The procedure to apply WDO for PV parameter estimation is discussed in the following.

Step 1: *Initialization of air parcels*: The PV parameters R_{P1}, R_{P2}, I_{01}, I_{02}, $I_{03}, n_1 V_T, n_2 V_T$, $n_3 V_T$, and I_{irr} are initialized inside the solution space and similarly,

the WDO parameters like *N-iter* and population size are declared.

Step 2: *Air parcel and pressure evaluation*: The air parcels are evaluated for their pressure and its movement is weighed. The fitness function used for evaluation is given in (7) and (8). Note that the parameters are permitted only to move in the velocity range [-1, 1] and its mapping can be verified by using the

$$x_j^k = (\text{Max}_j - \text{Min}_j) \times \left(\left(\frac{y_j^k + 1}{2} \right) + \text{Min}_j \right). \tag{19}$$

Step 3: *Rank update:* Since PV parameter estimation is a minimization objective function, ascending order-based rank evaluation is followed to identify the optimal particle with best fitness.

Step 4: *Evaluation for P_{best} and G_{best}*: The air parcels with optimal pressure value at the end of each iteration is identified as current best solution and P_{best} as the air parcel with overall best fitness is termed as global best solution G_{best}. Note that the global best solution is always updated at the end of each iteration to represent the optimal value.

Step 5: *Velocity and position update*: Perform velocity and position update using (17) and (19). Note that CMAES is called here to generate the coefficients for position and velocity update. During evaluation, it is important to bring the air parcels if the boundary limits are breached, hence, the following formulae is used to serve for the purpose:

$$u_{\text{new}_j}^p = \begin{cases} u_{\text{max}} & \text{if } u_{\text{new}j}^k > u_{\text{max}} \\ -u_{\text{max}} & \text{if } u_{\text{new}j}^k < -u_{\text{max}} \end{cases}. \tag{20}$$

Step 6: *Stopping criterion:* Step 2 to 5 is continuously repeated for 1000 iterations and the optimal values pertinent to OPV parameters are displayed. For better understanding with the application of WDO with OPV parameter extraction, the flowchart is presented in Fig. 4.

C. Case Study Illustrating the Compatibility of WDO for OPV Parameter Estimation

To justify the applicability of WDO for OPV parameter estimation, a case study on velocity update with all 9 dimensions (R_{P1}, R_{P2}, I_{01}, I_{02}, I_{03}, n_1, n_2, n_3, and I_{irr}) is carried out. Furthermore, the velocity consumed by all dimensions is captured at the end of 15 consecutive iterations using MATLAB to forecast the suitability of proposed algorithm. Initial velocity consumed the samples and its movement is presented in contour chart, as shown in Fig. 5(a). Note that the samples are well distributed across all regions inside the search space. The contour plot presented in Fig. 5(a) acknowledges the randomness in initialization with the air samples. Similar representation of samples at the end of 15th, 30th, and 45th iterations are presented in Fig. 5(b)–(d), respectively. From
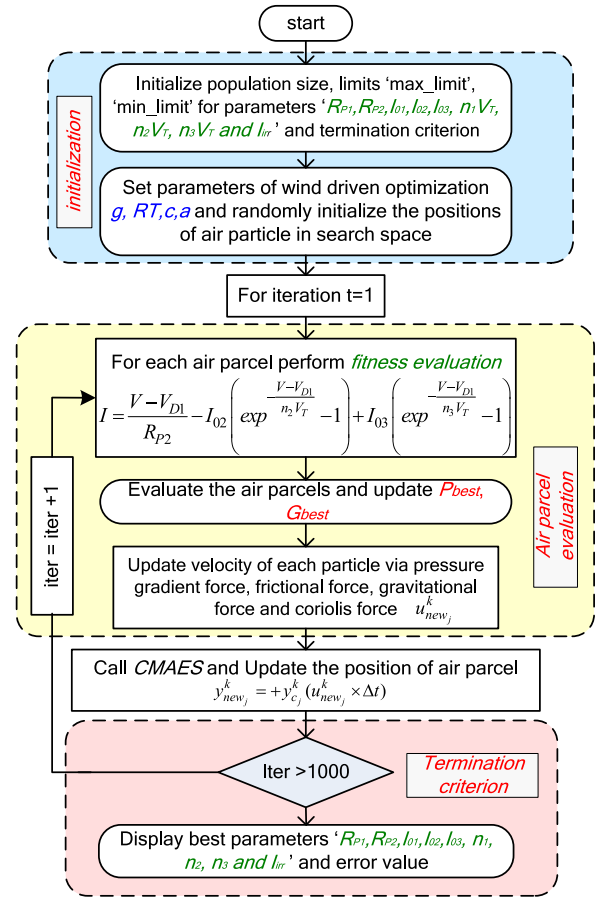

Fig. 4.　Flowchart for WDO - OPV parameter estimation.

the sample movement, it is interesting to note that except R_{P2} and I_{01}, all remaining dimensions have obtained the global vicinity at the end of 30th iteration. Furthermore, the influence of R_{P1}, I_{02}, $I_{03}, n_1 V_T, n_2 V_T$, $n_3 V_T$, and I_{irr} via gravitational velocity and Coriolis velocity update has made the other two dimensions converge which is clearly visible in 45th iteration, as shown in Fig. 5(d). Moreover, the adaptive velocity update followed by each dimension is a notable advantage with the WDO method. Meanwhile, the air samples consuming velocity closely to 1 are clearly visible in the contour plot at the end of 40th iteration. This shows the successful exhibition on application of WDO to OPV parameter estimation. Besides, it is one of the most needed merits of WDO to suit for nonlinear optimization problems. In general, very few metaheuristic algorithms has the ability to suit for multidimensional nonlinear problems say; flower pollination algorithm, fireworks algorithm, particle swarm optimization, and its predecessors. However, their procedural complexity and parameter tuning become a major hindrance to apply for multidimensional problems. Thus, WDO algorithm has proved to create arbitrariness for multidimensional problems and its success of hasty convergence is verified. Few notable advantages for OPV parameter estimation using the WDO are i) adaptive velocity generation, ii) hasty
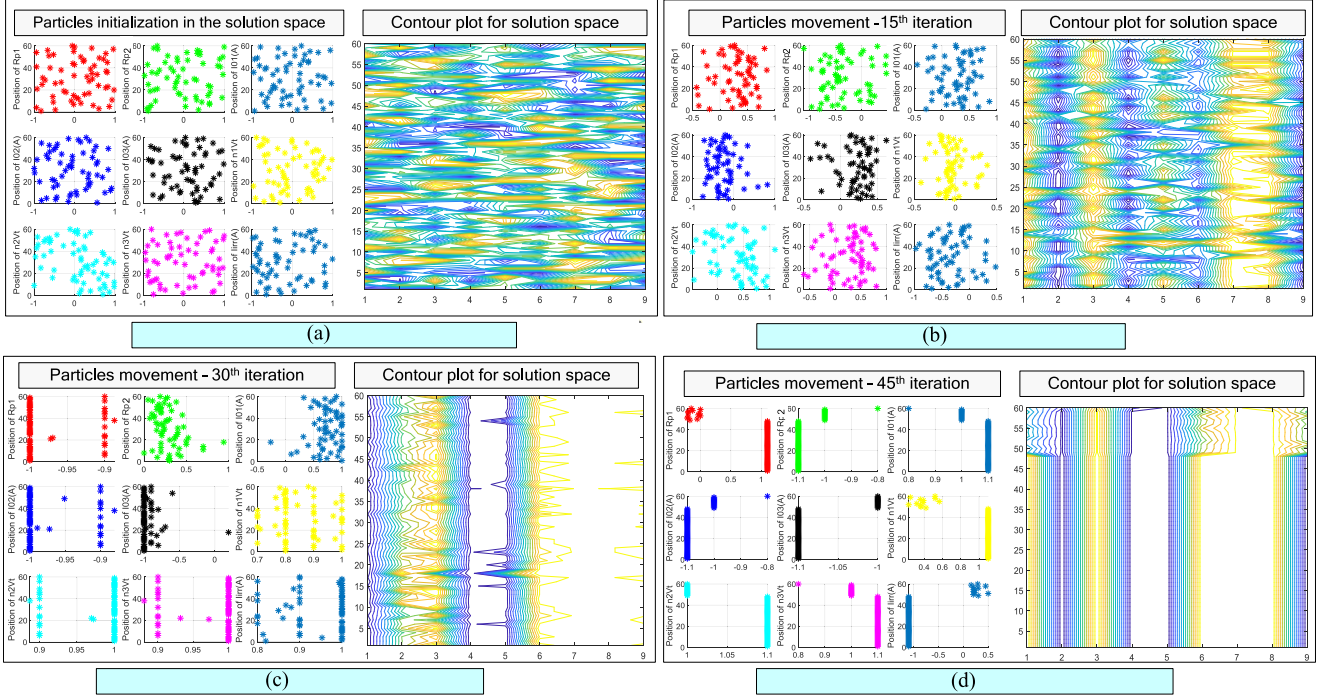
Fig. 5. Velocity update of $R_{P1}, R_{P2}, I_{01}, I_{02}, I_{03}, n_1V_T, n_2V_T, n_3V_T,$ and I_{irr} in the search space. (a) WDO particle initialization. (b) WDO particle movement in 15th iteration. (c) WDO particle movement in 30th iteration. (d) WDO particle movement in 45th iteration.

convergence, iii) ability to handle multidimensional nonlinearity, and iv) exhibition of excellent tradeoff between exploration and exploitation.

IV. RESULTS AND DISCUSSIONS

The simulation trials for the application of WDO for organic solar PV is performed in MATLAB. Detailed descriptions of materials used for the study is given in Section II. Further investigation on PV materials is avoided in this article since the primary scope of the work is to only obtain accurate PV parameters to model an OPV via electrical equivalent circuit. For the organic photovoltaic sample proposed in Section II [26], [28], *I–V* characteristics are annealed for temperature 120 °C, 150 °C, 180 °C, and 200 °C. Furthermore, the nature of change in *I–V* characteristics pertinent to each temperature is observed for various irradiation changes that include 10 mW/cm², 30 mW/cm², 50 mW/cm², 80 mW/cm², and 100 mW/cm². Data to plot the actual *I–V* characteristics are referred and taken from [26]. In this article, curve fits for these curves are performed and the parameters ($R_{P1}, R_{P2}, I_{01}, I_{02}, I_{03}, n_1V_T, n_2V_T, n_3V_T,$ and I_{irr}) for optimization are determined using WDO algorithm. The limits programmed for the aforementioned parameters are given in the following: $1000 < R_{P1} < 1 E + 06$, $10 < R_{P2} < 500$, $0.01 < I_{01} < 1 E - 09$, $0.01 < I_{02} < 1 E - 09$, $0.01 < I_{03} < 1 E - 09$, $0.01 < n_1V_T < 0.5$, $0.01 < n_2V_T < 0.5$, $0.01 < n_3V_T < 0.5$, and $0.001 < I_{irr} < 0.01$.

A. Curve Fit Analysis of Nonannealed Sample at 100 mW/cm²

To identify the closeness between the actual and simulated data, the curve fit analysis for the nonannealed sample (nalv100)
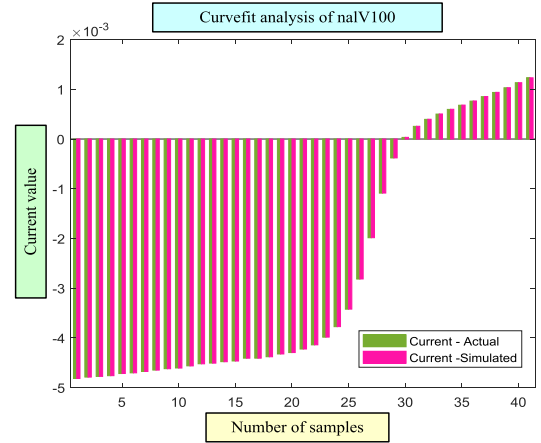

Fig. 6. Curve fit analysis for nalV100.

at 100 mW/cm² is performed and its current values are plotted, as shown in Fig. 6. From the plotted characteristics, the difference between actual and simulated values is found to be negligible. Furthermore, the accuracy of WDO algorithm to arrive at the accurate OPV parameters is one of the key reasons for the successful simulations. OPV parameters corresponding to nalv100 obtained via WDO is tabulated in Table I. Since the data of OPV is only available for 100 mW/cm² in literature, the comparison of OPV - nav100 with existing literature [26] annealed at various temperatures 120 °C, 150 °C, 180 °C, and 200 °C are presented in Appendix. Relative error evaluation with the actual and simulated eventually concludes the importance of WDO in multidimensional nonlinear problems. Perhaps, the

TABLE I
OPV PARAMETERS ESTIMATED FOR NAV100 AT 100 MW/CM²

Parameters	Proposed	[26]
100 mW/cm²		
'R_{P1}'(Ω)	9.74 E+4	1.87E+03
'R_{P2}'(Ω)	20.54	5.60E+02
'I_{01}' (A)	4.63 E-4	1.33E-05
'I_{02}'(A)	3.17 E-4	2.42E-04
'I_{03}'(A)	2.05 E-4	2.17E-09
'$n_1 V_T$'(V)	12.85E-02	7.73E-02
'$n_2 V_T$' (V)	12.76E-02	4.36E-02
'$n_3 V_T$' (V)	12.53E-02	5.58E-02
I_{irr} (A)	4.30 E-03	4.35E-03
RMSE	2.42 E-12	8.01E-11

TABLE II
OPV PARAMETERS ESTIMATED FOR VARIOUS IRRADIATION CONDITIONS AT
TEMPERATURES 120 °C, 150 °C, 180 °C, AND 200 °C

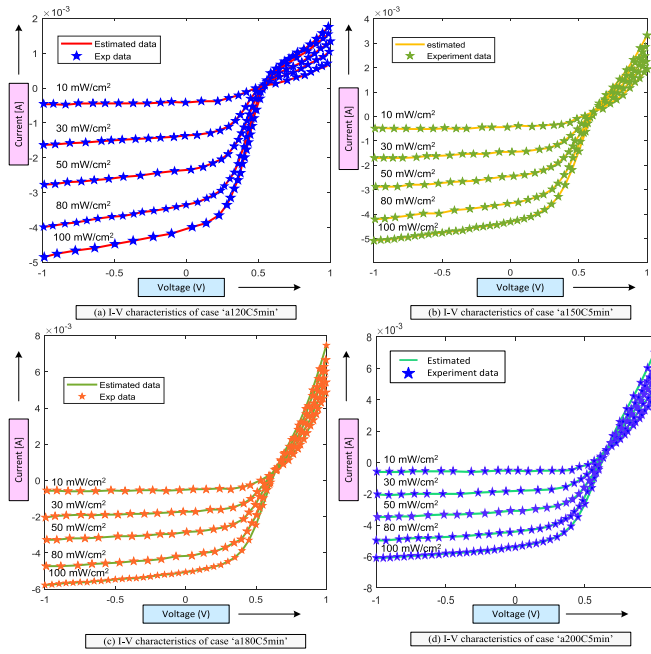| Parameters	a120C5min	a150C5min	a180C5min	a200C5min
100 mW/cm²				
'R_{P1}'(Ω)	1.53E+05	1.02E+05	5.38E+05	1.72E+05
'R_{P2}'(Ω)	20.82	156.25	50	18.092
'I_{01}' (A)	3.07E-04	4.50E-04	3.87E-05	3.15E-04
'I_{02}'(A)	1.04E-08	1.65E-08	3.55E-04	0.01
'I_{03}' (A)	5.00E-04	1.29E-08	0.0012	1.04E-08
'$n_1 V_T$'(V)	0.1285	0.1283	0.1016	0.2253
'$n_2 V_T$' (V)	0.0485	0.1182	0.2569	0.2564
'$n_3 V_T$' (V)	0.0979	0.0985	0.2569	0.0257
I_{irr} (A)	0.0045	0.005	0.0057	0.0058
RMSE	4.11E-12	6.17E-12	1.33E-14	2.25E-13
80 mW/cm²				
'R_{P1}'(Ω)	8.95E+04	5.62E+05	4.90E+05	4.35E+05
'R_{P2}'(Ω)	30.6	50.54	46.82	39.6
'I_{01}' (A)	5.18E-04	1.03E-03	1.85E-08	8.67E-04
'I_{02}'(A)	3.11E-04	5.19E-04	7.88E-08	4.51E-04
'I_{03}' (A)	2.23E-04	1.26E-08	2.58E-04	2.34E-04
'$n_1 V_T$'(V)	0.1625	0.1485	0.0257	0.1285
'$n_2 V_T$' (V)	0.1275	0.1105	0.0735	0.1835
'$n_3 V_T$' (V)	0.1835	0.1995	0.1285	0.1555
I_{irr} (A)	0.0035	0.0032	0.0047	0.0041
RMSE	3.78E-12	6.02E-13	2.91E-13	2.55E-13
50 mW/cm²				
'R_{P1}'(Ω)	9.82E+04	4.78E+05	4.85E+05	2.35E+05
'R_{P2}'(Ω)	250.531	36.5	166.7145	52.63
'I_{01}' (A)	9.85E-04	9.50E-04	7.24E-06	1.00E-08
'I_{02}'(A)	5.11E+08	1.04E-08	1.45E-08	3.62E-08
'I_{03}' (A)	1.76E-05	6.06E-05	1.01E-08	0.0084
'$n_1 V_T$'(V)	0.1238	0.0257	0.0257	0.0638
'$n_2 V_T$' (V)	0.1285	0.1285	0.1285	0.1002
'$n_3 V_T$' (V)	0.1284	0.1285	0.1285	0.0881
I_{irr} (A)	0.0422	0.046	0.0385	0.036
RMSE	4.03E-12	8.85E-13	4.80E-13	3.73E-12
30 mW/cm²				
'R_{P1}'(Ω)	3.58E+04	8.79E+04	9.52E+04	1.03E+05
'R_{P2}'(Ω)	455.6	432.05	21.06	35.62
'I_{01}' (A)	8.60E-04	1.67E-07	1.07E-04	5.06E-08
'I_{02}'(A)	1.34E-08	3.30E-08	3.91E-04	1.67E-08
'I_{03}' (A)	1.02E-08	2.08E-08	1.03E-08	3.66E-04
'$n_1 V_T$'(V)	0.1028	0.0257	0.1242	0.0257
'$n_2 V_T$' (V)	0.1935	0.1762	0.0487	0.1375
'$n_3 V_T$' (V)	0.1285	0.1272	0.0487	0.1285
I_{irr} (A)	0.05	0.0128	0.001	0.05
RMSE	3.12E-11	1.12E-11	1.23E-11	3.29E-11
10 mW/cm²				
'R_{P1}'(Ω)	1.03E+05	1.80E+04	3.52E+04	4.52E+04
'R_{P2}'(Ω)	35.8	28.6	218.07	21.53
'I_{01}' (A)	1.38E-03	1.08E-03	5.63E-03	2.34E-03
'I_{02}'(A)	1.06E-08	7.67E-05	1.34E-08	5.30E-09
'I_{03}' (A)	0.01	5.64E-05	5.80E-09	1.44E-04
'$n_1 V_T$'(V)	0.11285	0.127	0.1185	0.1075
'$n_2 V_T$' (V)	0.1785	0.1325	0.0853	0.1285
'$n_3 V_T$' (V)	0.1285	0.1342	0.0965	0.11485
I_{irr} (A)	0.05	0.02	0.03	0.05
RMSE	4.26E-10	3.77E-10	1.09E-10	1.84E-10

Fig. 7. Simulated *I–V* characteristics for OPV sample at various irradiation conditions.

tradeoff between the exploration and exploitation in handling the control variables with WDO has resulted better results for OPV parameter estimation.

B. Simulation Analysis of Annealed OPV Sample at Different Temperatures

With enough potential exhibited to produce the exact curve fit for nonannealed samples, the simulation analysis is extended for annealed samples as well. For analysis, the OPV sampled treated for 120 °C, 150 °C, 180 °C, and 200 °C at irradiation levels 10 mW/cm², 30 mW/cm², 50 mW/cm², 80 mW/cm², and 100 mW/cm². This analysis demands critical examination since extracting accurate PV parameters at almost dark conditions like 10 mW/cm² is really challenging for any optimization techniques. Furthermore, matching current value to reproduce exact *I–V* characteristics necessitates explicit exploration and exploitation in the dimensions of optimization constraints. Besides, the kink effect in OPV *I–V* characteristics adds even more complexity to arrive at actual and accurate PV parameters. The

actual and simulated data for various temperature corresponding to different irradiations can be seen in Fig. 7. Furthermore, the PV parameters arrived pertinent to simulation at different temperature and irradiation conditions are presented in Table II. Various observations with the simulations performed with OPV are summarized in the following.

APPENDIX

COMPARISON OF OPV PARAMETERS ANNEALED FOR TEMPERATURES 120 °C, 150 °C, 180 °C, AND 200 °C AT 100 MW/CM^2.

Parameters	a120C5min		a150C5min		a180C5min		a200C5min	
	Proposed	[26]	Proposed	[26]	Proposed	[26]	Proposed	[26]
'R_{P1}'(Ω)	1.53E+05	1.28E+03	1.02E+05	1.33E+03	5.38E+05	1.43E+03	1.72E+05	1.44E+03
'R_{P2}'(Ω)	20.82	3.72E+02	156.25	5.66E+02	50	5.49E+02	18.092	4.77E+01
'I_{01}' (A)	3.07E−04	6.59E−06	4.50E−04	2.04E−05	3.87E−05	1.65E−05	3.15E−04	2.93E−05
'I_{02}'(A)	1.04E−08	3.73E−04	1.65E−08	4.42E−04	3.55E−04	6.44E−04	1.00E−03	9.02E−04
'I_{03}' (A)	5.00E−04	4.69E−06	1.29E−08	8.62E−04	1.20E−03	3.37E−03	1.04E−08	8.73E−07
'$n_1 V_T$'(V)	12.85E−02	8.34E−02	12.83E−02	1.12E−01	1.01E−01	1.08E−01	2.25E−01	1.20E−01
'$n_2 V_T$' (V)	4.85 E−02	3.85E−02	11.82E−02	3.49E−02	2.56E−01	2.29E−02	2.56E−01	2.77E−02
'$n_3 V_T$' (V)	9.79 E−02	1.09E−01	9.85E−02	2.61E−01	2.56E−01	2.72E−01	2.57E−02	4.74E−02
I_{irr} (A)	4.50E−03	4.17E−03	5.00E−03	4.40E−03	5.70E−03	5.11E−03	5.80E−03	5.45E−03
RMSE	4.11E-12	1.25E−10	6.17E-12	1.36E−10	1.33E−14	5.35E−10	2.25E-13	7.85E−10

1) Estimating PV parameters for samples annealed at 180 °C and 200 °C is really complex since the nonlinearity is found to be very high. Particularly, the kink effect at higher irradiations makes it extremely tough to simulate. Despite the fact, WDO has given accurate PV parameters at all levels of irradiations to reproduce the exact *I–V* characteristics of OPV.

2) The kink effect of annealed samples at 180 °C and 200 °C is found to be negligible and it resembles the characteristics of nonorganic c-Si PV cells, thus making PV parameter estimation easier comparatively.

3) Exploration and exploitation ability and the balance between them in WDO has made easier to arrive at OPV parameters for all irradiation conditions.

4) The velocity and position update process has a notable role in WDO parameter estimation to reproduce exact *I–V* characteristics of OPV.

5) From the tabulated values of OPV, the mean square error is found almost negligible and more accurate compared to the results proposed in [28].

C. IAE Analysis of OPV Sample Performed at 100 mW/cm^2

Evaluation of OPV parameter estimation via individual absolute error is an obligatory requirement to evaluate the results of WDO. For this analysis, the curve fit of OPV sample pertinent to annealed temperatures 120 °C, 150 °C, 180 °C, and 200 °C; and nonannealed values only at irradiation 100 mW/cm^2 is considered. The extracted error curve for absolute error analysis is presented in Fig. 8. From the analysis, it can be found that error values are almost in the range of 10^{-6}, which is highly accurate to reproduce the actual points of OPV *I–V* characteristics. More importantly, the precise values obtained with inclusion of kink effect should be valued more. Irrespective of various dimensions, WDO has produced accurate OPV parameters, which is clear exhibition of its balance in exploration and exploitation ability. Besides, the error values are almost the same for other irradiations as well. Formulae used for evaluating absolute error is given as follows:

$$IAE = |I_{\text{actual}} - I_{\text{simulated}}|. \quad (21)$$
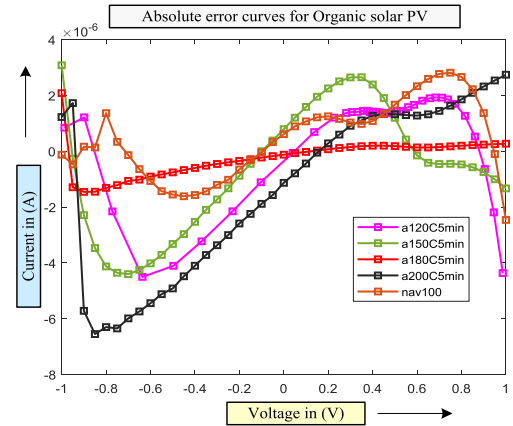
Fig. 8. Individual absolute error analysis for OPV sample at 100 mW/cm^2.

V. CONCLUSION

A recent nature-inspired wind-driven optimization have been applied for multidimensional organic solar PV parameter estimation problem in this article. Based on the extensive analysis performed, the following conclusions are likely to be summarized.

1) Existence of kink effect in the *I–V* characteristics is one of the major challenges in OPV and the used three-diode electrical equivalent circuit is highly efficient to handle the nonlinearity.

2) Parameters found via WDO method are precise and accurate to obtain exact *I–V* characteristics.

3) Analysis on error values and convergence characteristics has evidenced the justification to use WDO for PV parameter estimation. Particularly, the attainment of fitness (mean square error) in 10^{-12} range has gained momentary attraction to make WDO as one of the best optimization techniques to apply for nonlinear optimization problems.

4) Availability of Coriolis and gravitational forces navigates the air parcels towards global regions in quick succession.

REFERENCES

[1] C. S. Solanki, "Solar photovoltaics: Fundamentals, technologies, and applications," Phi Learn. Pvt. Ltd., May 2015.

[2] M. A. Green, K. Emery, Y. Hishikawa, W. Warta, and E. D. Dunlop, "Solar cell efficiency tables (version 47)," *Prog. Photovolt. Res. Appl.*, vol. 24, no. 1, pp. 3–11, Jan. 2016, doi: 10.1002/pip.2728.

[3] J. Kong *et al.*, "Long-term stable polymer solar cells with significantly reduced burn-in loss," *Nat. Commun.*, vol. 5, no. 1, pp. 1–8, Dec. 2014, doi: 10.1038/ncomms6688.

[4] A. Wagenpfahl, D. Rauh, M. Binder, C. Deibel, and V. Dyakonov, "S-shaped current-voltage characteristics of organic solar devices," *Phys. Rev. B - Condens. Matter Mater. Phys.*, vol. 82, no. 11, pp. 1–8, Sep. 2010.

[5] M. B. Prince, "Silicon solar energy converters," *J. Appl. Phys.*, vol. 26, no. 5, pp. 534–540, May 2004, doi: 10.1063/1.1722034.

[6] A. Askarzadeh and A. Rezazadeh, "Extraction of maximum power point in solar cells using bird mating optimizer-based parameters identification approach," *Sol. Energy*, vol. 90, pp. 123–133, Apr. 2013, doi: 10.1016/j.solener.2013.01.010.

[7] T. S. Babu, J. P. Ram, K. Sangeetha, A. Laudani, and N. Rajasekar, "Parameter extraction of two diode solar PV model using fireworks algorithm," *Sol. Energy*, vol. 140, pp. 265–276, 2016, doi: 10.1016/j.solener.2016.10.044.

[8] K. Ishaque, Z. Salam, S. Mekhilef, and A. Shamsudin, "Parameter extraction of solar photovoltaic modules using penalty-based differential evolution," *Appl. Energy*, vol. 99, pp. 297–308, Nov. 2012, doi: 10.1016/j.apenergy.2012.05.017.

[9] B. Subudhi and R. Pradhan, "Bacterial foraging optimization approach to parameter extraction of a photovoltaic module," *IEEE Trans. Sustain. Energy*, vol. 9, no. 1, pp. 381–389, Jan. 2018, doi: 10.1109/TSTE.2017.2736060.

[10] D. F. Alam, D. A. Yousri, and M. B. Eteiba, "Flower pollination algorithm based solar PV parameter estimation," *Energy Convers. Manage.*, vol. 101, pp. 410–422, Jun. 2015.

[11] J. P. Ram, T. S. Babu, T. Dragicevic, and N. Rajasekar, "A new hybrid bee pollinator flower pollination algorithm for solar PV parameter estimation," *Energy Convers. Manage.*, vol. 135, pp. 463–476, 2017, doi: 10.1016/j.enconman.2016.12.082.

[12] D. S. Pillai and N. Rajasekar, "Metaheuristic algorithms for PV parameter identification: A comprehensive review with an application to threshold setting for fault detection in PV systems," *Renewable Sustain. Energy Rev.*, vol. 82, pp. 3503–3525, Jan./Feb. 2018.

[13] A. Ortiz-Conde, O. Trejo, and F. J. Garcia-Sanchez, "Direct extraction of solar cell model parameters using optimization methods," in *Proc. IEEE Latin Amer. Electron Devices Conf.*, 2021, pp. 1–6, doi: 10.1109/LAEDC51812.2021.9437951.

[14] O. J. Sandberg, M. Nyman, and R. Österbacka, "Effect of contacts in organic bulk heterojunction solar cells," *Phys. Rev. Appl.*, vol. 1, no. 2, pp. 1–15, Mar. 2014, doi: 10.1103/PhysRevApplied.1.024003.

[15] G. Del Pozo, B. Romero, and B. Arredondo, "Evolution with annealing of solar cell parameters modeling the S-shape of the current-voltage characteristic," *Sol. Energy Mater. Sol. Cells*, vol. 104, pp. 81–86, Sep. 2012, doi: 10.1016/j.solmat.2012.04.048.

[16] B. Mazhari, "An improved solar cell circuit model for organic solar cells," *Sol. Energy Mater. Sol. Cells*, vol. 90, no. 7/8, pp. 1021–1033, May 2006, doi: 10.1016/j.solmat.2005.05.017.

[17] A. Cheknane, H. S. Hilal, F. Djeffal, B. Benyoucef, and J. P. Charles, "An equivalent circuit approach to organic solar cell modelling," *Microelectron. J.*, vol. 39, no. 10, pp. 1173–1180, Oct. 2008, doi: 10.1016/j.mejo.2008.01.053.

[18] F. A. De Castro, J. Heier, F. Nesch, and R. Hany, "Origin of the kink in current-density versus voltage curves and efficiency enhancement of polymer-C 60 heterojunction solar cells," *IEEE J. Sel. Topics Quantum Electron.*, vol. 16, no. 6, pp. 1690–1699, Nov. 2010, doi: 10.1109/JSTQE.2010.2040807.

[19] B. Romero, G. del Pozo, and B. Arredondo, "Exact analytical solution of a two diode circuit model for organic solar cells showing S-shape using lambert W-functions," *Sol. Energy*, vol. 86, no. 10, pp. 3026–3029, Oct. 2012, doi: 10.1016/j.solener.2012.07.010.

[20] F. J. García-Sánchez, D. Lugo-Muñoz, J. Muci, and A. Ortiz-Conde, "Lumped parameter modeling of organic solar cells' S-shaped I–V characteristics," *IEEE J. Photovolt.*, vol. 3, no. 1, pp. 330–335, Jan. 2013, doi: 10.1109/JPHOTOV.2012.2219503.

[21] D. S. H. Chan and J. C. H. Phang, "Analytical methods for the extraction of solar-cell Single-and double-diode model parameters from I–V characteristics," *IEEE Trans. Electron Devices*, vol. 34, no. 2, pp. 286–293, Feb. 1987, doi: 10.1109/T-ED.1987.22920.

[22] W. De Soto, S. A. Klein, and W. A. Beckman, "Improvement and validation of a model for photovoltaic array performance," *Sol. Energy*, vol. 80, no. 1, pp. 78–88, Jan. 2006, doi: 10.1016/j.solener.2005.06.010.

[23] A. Ortiz-Conde, F. J. García Sánchez, and J. Muci, "Exact analytical solutions of the forward non-ideal diode equation with series and shunt parasitic resistances," *Solid. State. Electron.*, vol. 44, no. 10, pp. 1861–1864, Oct. 2000, doi: 10.1016/S0038-1101(00)00132-5.

[24] F. García-Sánchez *et al.*, "Modelling solar cell S-shaped I–V characteristics with DC lumped-parameter equivalent circuits a review," *Facta Univ. - Ser. Electron. Energ.*, vol. 30, no. 3, pp. 327–350, 2017, doi: 10.2298/FUEE1703327G.

[25] A. Jain and A. Kapoor, "Exact analytical solutions of the parameters of real solar cells using lambert W-function," *Sol. Energy Mater. Sol. Cells*, vol. 81, no. 2, pp. 269–277, Feb. 2004, doi: 10.1016/j.solmat.2003.11.018.

[26] F. De Castro, A. Laudani, F. R. Fulginei, and A. Salvini, "An in-depth analysis of the modelling of organic solar cells using multiple-diode circuits," *Sol. Energy*, vol. 135, pp. 590–597, Oct. 2016, doi: 10.1016/j.solener.2016.06.033.

[27] P. J. Roland, K. P. Bhandari, and R. J. Ellingson, "Electronic circuit model for evaluating S-kink distorted current-voltage curves," in *Proc. IEEE 43rd Photovolt. Specialists Conf.*, 2016, pp. 3091–3094, doi: 10.1109/PVSC.2016.7750234.

[28] A. Laudani, F. R. Fulginei, F. De Castro, and A. Salvini, "Irradiance intensity dependence of the lumped parameters of the three-diodes model for organic solar cells," *Sol. Energy*, vol. 163, pp. 526–536, Mar. 2018, doi: 10.1016/j.solener.2018.02.032.

[29] D. Mathew *et al.*, "Wind-driven optimization technique for estimation of solar photovoltaic parameters," *IEEE J. Photovolt.*, vol. 8, no. 1, pp. 248–256, Jan. 2018, doi: 10.1109/JPHOTOV.2017.2769000.

[30] Z. Bayraktar, M. Komurcu, J. A. Bossard, and D. H. Werner, "The wind driven optimization technique and its application in electromagnetics," *IEEE Trans. Antennas Propag.*, vol. 61, no. 5, pp. 2745–2757, May 2013, doi: 10.1109/TAP.2013.2238654.

[31] F. A. Castro *et al.*, "Nanostructured organic layers via polymer demixing for interface-enhanced photovoltaic cells," *Chem. Mater.*, vol. 18, no. 23, pp. 5504–5509, Nov. 2006, doi: 10.1021/cm061660r.

[32] K. Tada, "Validation of opposed two-diode equivalent-circuit model for S-shaped characteristic in polymer photocell by low-light characterization," *Org. Electron.*, vol. 40, pp. 8–12, Jan. 2017, doi: 10.1016/j.orgel.2016.10.031.